Global variability of precipitation according to the Tropical Rainfall Measuring Mission

Ziad S. Haddad and Jonathan P. Meagher
Jet Propulsion Laboratory, California Institute of Technology, Pasadena, California, USA

Robert F. Adler and Eric A. Smith
NASA Goddard Space Flight Center, Greenbelt, Maryland, USA

Eastwood Im and Stephen L. Durden
Jet Propulsion Laboratory, California Institute of Technology, Pasadena, California, USA

Received 5 February 2004; revised 30 April 2004; accepted 25 June 2004; published 11 September 2004.

[1] Numerous studies have documented the effect of El Niño-Southern Oscillation (ENSO) on rainfall in many regions of the globe. The question of whether ENSO is the single most important factor in interannual rainfall variability has received less attention, mostly because the kind of data that would be required to make such an assessment were simply not available. Until 1979 the evidence linking El Niño with changes in rainfall around the world came from rain gauges measuring precipitation over land masses and a handful of islands. From 1980 until the launch of the Tropical Rainfall Measuring Mission (TRMM) in November 1997 the remote sensing evidence was confined to ocean rainfall because of the very poor sensitivity of the instruments over land. In this paper we summarize the results of a principal component analysis of TRMM's 60-month (January 1998 to December 2002) global land and ocean remote-sensing record of monthly rainfall accumulations. Contrary to the first principal component of the rainfall itself, the first three indices of the anomaly are most sensitive to precipitation over the ocean rather than over the land. With the help of archived surface station data the first TRMM rain anomaly index is extended back several decades. Comparison of the extended index with the Southern Oscillation Index confirms that the first principal component of the rainfall anomaly is strongly correlated with the ENSO indices. *INDEX TERMS:* 1640 Global Change: Remote sensing; 1854 Hydrology: Precipitation (3354); 3360 Meteorology and Atmospheric Dynamics: Remote sensing; *KEYWORDS:* rainfall

Citation: Haddad, Z. S., J. P. Meagher, R. F. Adler, E. A. Smith, E. Im, and S. L. Durden (2004), Global variability of precipitation according to the Tropical Rainfall Measuring Mission, *J. Geophys. Res.*, *109*, D17103, doi:10.1029/2004JD004607.

1. Background

[2] Numerous studies have documented the link between El Niño-Southern Oscillation (ENSO) and rainfall in many regions of the globe, associating the warm phase with drought conditions in some cases, unusually abundant precipitation in others. The most extensive and detailed study of this kind is undoubtedly *Ropelewski and Halpert*'s [1987, 1988], in which the change in the rainfall sampled over land and island stations within several regions around the globe is carefully analyzed depending on the prevailing ENSO conditions. Indeed, consistent correlations are found between the rain anomaly and the ENSO phase in most of the regions considered [*Ropelewski and Halpert*, 1987]. One could contemplate synthesizing these observations into a global ENSO precipitation index, which would be calculated by adding the rainfall anomalies in all areas which experience excess rain during warm ENSO phases and subtracting the anomaly in those areas which experience a deficit. The problem with such a proposition is that regions which experience excess rain during warm phases do not always experience rain deficits during cold phases and vice versa, as *Ropelewski and Halpert* [1988] observed. In other words, the maps of the rainfall anomalies during warm and cold ENSO phases do not appear to be mirror images of one another. An equally serious problem with the proposition of subtracting deficit areas from excess areas is that, by subjectively selecting only those areas which have a consistently sustained correlation with ENSO, one would be ignoring those regions which are less significantly affected by the phenomenon, and which could be responsible for a large proportion of the global rainfall variability. This problem was addressed by the objective study of *Dai et al.* [1997], in which a global set of yearly rainfall compiled from land/island station data from 1900 to 1988, was analyzed. After subtracting from the values for each station their mean from 1900 to 1988, and normalizing by the

0148-0227/04/2004JD004607$09.00

corresponding standard deviation to prevent regions with a large overall variation from overwhelming the subtle change in regions with low rainfall, a principal component analysis of the resulting normalized anomaly was performed. Dai et al. found that the first principal component of the normalized annual rain anomaly over the period 1900–1988 was very well correlated indeed with the bimonthly average sea-surface temperature anomaly over the equatorial Pacific. While these results are based exclusively on land/island station data which leave vast expanses of ocean unrepresented, they are compelling indicators that ENSO is a very important factor in the variability of rainfall. Thus the accumulated evidence begs the question: how can one objectively quantify the importance of ENSO in the global (land and ocean) variability of surface rainfall? Or, in other words, without any a priori awareness of ENSO, is it possible to examine the rainfall remote sensing record and condense its overall variability into a simple metric, then ask with what physical process this metric is most correlated?

[3] Until the work of *Arkin* [1979] and *Xie and Arkin* [1997] and that of *Adler et al.* [1993] and *Huffman et al.* [1997], this question had remained unaddressed largely because the systems required to monitor precipitation over the oceans simply did not exist. This dire situation changed dramatically in the 1980s with the availability of data from low-Earth-orbiting multiple-frequency microwave radiometers such as the Special Sensor Microwave Imagers (SSMI), and from geostationary visible/infrared (Vis/IR) imagers. The latter are useful in the sense that they can gauge the height of the cloud tops (and hence, at least in convective systems, the depth of the clouds, and hence, allowing for a quite large uncertainty in one's estimates, the amount of rain which these clouds are producing [see *Arkin* [1979]], with frequent updates. With less frequent updates, the low-Earth-orbiting microwave radiometers provide a handful of radiances in which the surface emissivity effects and the competition between the absorption/emission and the scattering from rain and ice can be approximately sorted out to produce an estimate of the rainfall amount at rather poor resolution. Acknowledging the limitations of SSMI and geostationary IR imagers, *Adler et al.* [1993] sought to combine them in order to take advantage of the strengths of each and build a "merged" IR-SSMI/surface-gauge data set of truly global rainfall, the Global Precipitation Climatology Project (GPCP) [see *Huffman et al.*, 1997]. An "ENSO precipitation index" (ESPI) is currently calculated from GPCP, essentially by subtracting the precpitation anomaly over the region around the Maritime Continent (10°S–10°N × 90°E–150°W) from that over the eastern Pacific (10°S–10°N × 160°E–100°W); the exact boundaries of the boxes are "dynamically" calculated in real time to maximize the contrast. By design, ESPI correlates very well with the "El Niño" and "Southern Oscillation" indices [*Curtis and Adler*, 2000]. Going one step further, *Xie and Arkin* [1997] folded in numerical model predictions as well, and produced the "CMAP" global data set of monthly surface rainfall estimates from 1979 to 1995 on a 2.5° grid. Their maps of the seasonal difference (warm phase-cold phase) of the rainfall anomaly averaged over the 17 years of data incorporated in CMAP confirmed that many of the results of *Ropelewski and Halpert* [1987, 1988] and *Dai and Wigley*'s [2000] principal component analysis of the normalized annual rain anomaly yielded a 20-point time series (CMAP had by then been updated to 1998) which matches the Southern Oscillation Index (SOI) over that period remarkably well. Yet, as Dai and Wigley point out, Xie and Arkin's seasonal maps fail to show many of the well-documented ENSO features (notably over Australia and the western United States), a fact which they attribute to the small amplitude of the anomaly away from the tropics as well as to the shortness of the time series, and which prompted Dai and Wigley to analyze the "prenormalized" anomaly rather than the anomaly itself: Specifically, they divide the anomaly in each pixel by the 20-year standard deviation for that pixel, thus amplifying the smaller absolute anomaly values in the extratropical pixels and similarly attenuating those in the tropical pixels. While the procedure has its merits, one is still left wondering whether the data would still exhibit good correlation between the rain anomaly and ENSO if it were not prenormalized pixel by pixel. In addition, these first truly global results depend ultimately on the reliability of the sources of the data, namely the IR and SSMI estimates. As we have already noted, the former relies on the statistically derived correlation between cloud top heights and surface rain, which has a large intrinsic uncertainty and whose applicability depends on precipitation type. While SSMI is more directly sensitive to the rain itself, the poor resolution of the instrument forces one to make homogeneity assumptions about the precipitation which are likely to introduce large biases in the estimates (because the average rain quantities one would like to estimate are related in a very nonlinear way to the average radiances one measures). Most important, over land the relation between either the IR or the microwave radiances and the surface precipitation is tenuous at best.

2. Tropical Rainfall Measuring Mission Analysis

[4] It is precisely to remedy the shortcomings of these systems (their poor resolution and their lack of much direct sensitivity to the vertical structure of precipitation) that the Tropical Rainfall Measuring Mission (TRMM) was conceived and the TRMM satellite launched in November 1997 [*Simpson et al.*, 1988]. In addition to having a very low resolution-enhancing orbit (originally 350 km), TRMM's advantage is that it carries the first spaceborne precipitation-profiling radar (PR), in addition to a nine-channel microwave radiometer (TMI) and a visible/infrared imager. Although the clutter from the overwhelming surface echo severely limits the swath of the PR and therefore limits its ability to sample the precipitation as frequently as a radiometer, the vertical detail with which it can probe the atmosphere, its insensitivity to the characteristics of the surface, and its high horizontal resolution ($\simeq$4 km) make it an ideal instrument with which to "calibrate" the rain retrievals of the radiometer within the narrow common swath of the radar [*Haddad et al.*, 1997], and subsequently carry this calibration over to the TMI-only retrievals over the wide swath of the radiometer [*Adler et al.*, 2000].

[5] Of particular interest are the surface rainfall estimates produced by this "TRMM-combined" radar/radiometer algorithm from December 1997 until February 2003. These estimates, more specifically the ones produced by version 5

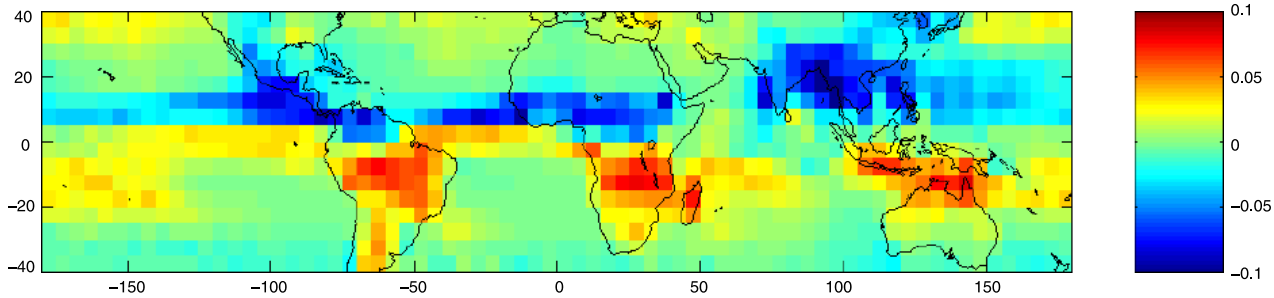

Figure 1. Coefficients of the first principal component of the TRMM-combined monthly rainfall averages for the 60 months of data from January 1998 to December 2002. (Note that there are $(80 \times 360)/(5 \times 5) = 1152$ pixels, so the reference value for the coefficients is $1/\sqrt{1152} \simeq 0.03$.)

of the algorithm (3B31v5 in the TRMM nomenclature) are available in the form of monthly rain maps over the region between 40°S and 40°N at a resolution of 5° × 5°. To synthesize the information in these maps objectively, we performed principal component analyses of the rainfall estimates and of their anomalies. Figure 1 illustrates the results. It displays the coefficients of the first principal component of the TRMM-combined monthly rainfall accumulation. As expected, the linear combination of pixels which captures the greatest share of the monthly variability (about 33%) in the rainfall is obtained essentially by subtracting the pixels with a November-to-April rain peak from the ones with a May-to-October rain peak, reflecting the simple fact that the seasons are indeed the major driver of the change in rainfall patterns from month to month. Much more interesting is the characterization of the variation of the monthly rain anomaly. Using the 60 months' worth of TRMM-combined data from January 1998 to December 2002 as the baseline to establish the monthly mean for each pixel, we performed a principal component analysis on the monthly TRMM-combined rain anomaly. The coefficients of the first three principal components PC_1,

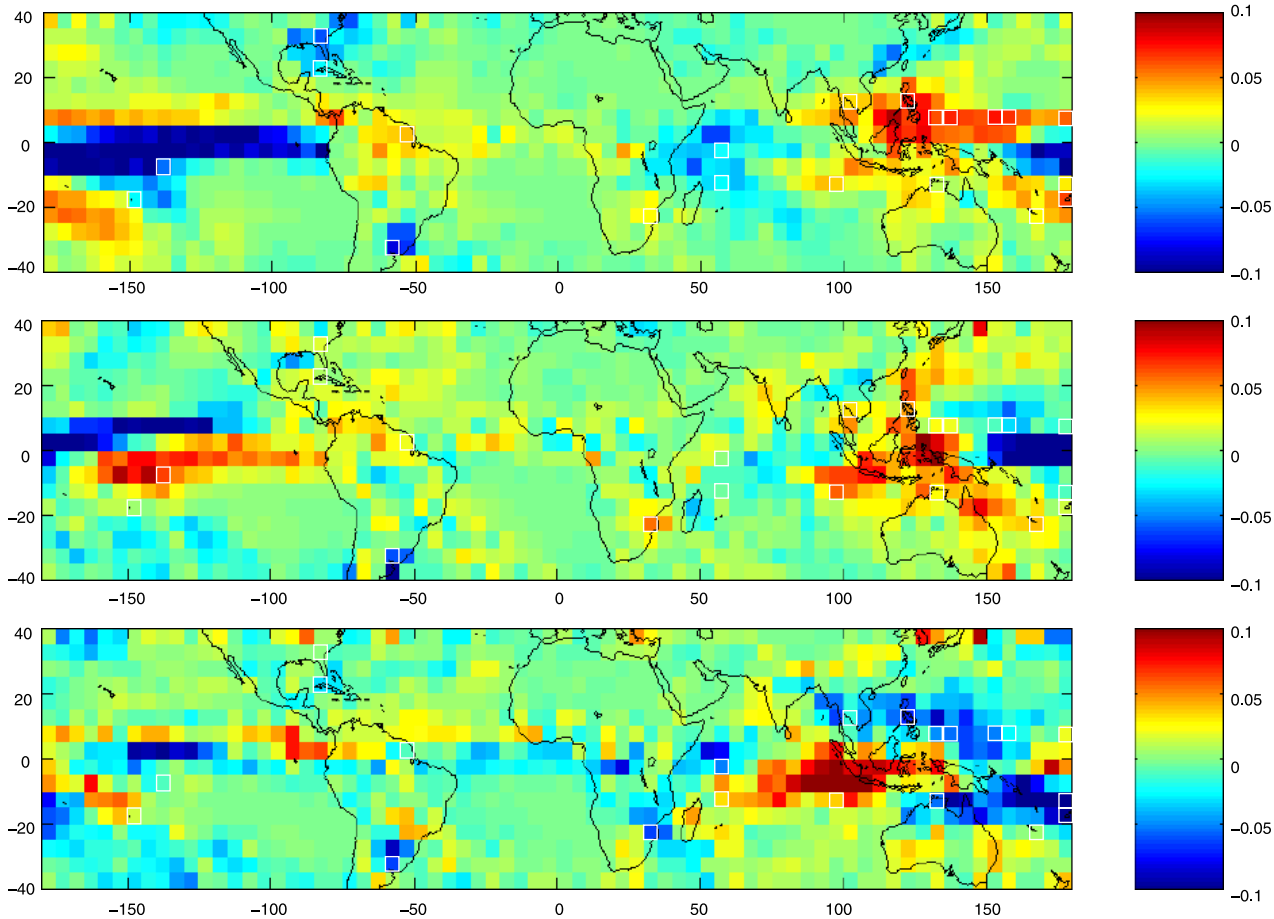

Figure 2. Coefficients of the first three principal components (top) PC_1, (middle) PC_2, and (bottom) PC_3 of the TRMM-combined monthly rainfall anomalies for the 60 months of data from January 1998 to December 2002 (the reference value for the coefficients is approximately 0.03).

Table 1. The 21 Pixels and Associated Stations and Their Corresponding Contribution to the Calculation of the Monthly Rainfall Anomaly Variability Index[a]

Longitude	Latitude	PC_1 Coefficient	GHCN Station	TRMM Pixel $\simeq a + b$ (GHCN Station) May to October (a, b)	TRMM Pixel $\simeq a + b$ (GHCN Station) November to April (a, b)
57.5°W	32.5°S	−0.083	Buenos Aires	(1.3, 74)	(0.83, 49)
122.5°E	12.5°N	0.078	Legaspi	(0.8, 59)	(0.56, −80)
152.5°E	7.5°N	0.078	Truk	(0.5, −43)	(0.58, −60)
137.5°E	7.5°N	0.073	Yap	(0.47, −63)	(0.78, −9)
157.5°E	7.5°N	0.071	Pohnpei	(0.54, −86)	(0.42, −85)
177.5°E	17.5°S	0.066	Nadi (Fiji)	(0.74,0)	(0.48, −45)
132.5°E	7.5°N	0.064	Koror (Palau)	(0.57, −65)	(0.37, −42)
82.5°E	27.5°N	−0.060	Jacksonville	(0.54, −15)	(1.0, 39)
172.5°E	7.5°N	0.049	Majuro	(0.48, −56)	(0.4, −32)
52.5°W	7.5°N	0.042	Cayenne	(0.43, −47)	(0.3, −42)
137.5°W	7.5°S	−0.039	Hiva Oa	(0.47, −33)	(0.37, −31)
97.5°E	12.5°S	0.038	Cocos Island	(0.57, −25)	(0.55, −38)
102.5°E	12.5°N	0.034	Bangkok	(0.5, 3)	(1.1, 27)
177.5°E	12.5°S	0.032	Rotuma (Fiji)	(0.83, −79)	(0.8, −72)
32.5°E	22.5°S	0.030	Inhambane	(1.0, 0)	(1.0, 0)
167.5°E	22.5°S	0.029	Noumea	(1.13, 7)	(0.52, −4)
57.5°E	12.5°S	−0.027	Agalega Island	(0.46, −12)	(0.4, −36)
147.5°W	17.5°S	−0.025	Tahiti	(1.1, 25)	(0.45, −16)
82.5°W	22.5°N	−0.025	Key West	(0.62, 11)	(1.0, 16)
57.5°E	2.5°S	−0.023	Mahe	(0.3, −12)	(0.33, −59)
132.5°E	12.5°S	0.013	Darwin	(0.72, 1)	(0.46, −51)

[a]GHCN, Global Historical Climatology Network; TRMM, Tropical Rainfall Measuring Mission.

PC_2, and PC_3 (ranked according to their variance in decreasing order) are shown in Figure 2. PC_1 accounts for about 14% of the variability, PC_2 accounts for another 7%, and PC_3 for a further 5%. As to the coefficients themselves, one readily notes that the variability of the rainfall anomaly is strongly sensitive to the precipitation over the oceans, in rather sharp contrast with the variability of the rainfall itself which, as Figure 1 shows, is more sensitive to continental rainfall. This is due to the more rapid and pronounced response of the continents to summer heating (winter cooling), which enhances (inhibits) the rain-producing convection. In contrast, the tropical Western Pacific and the equatorial Eastern Pacific have large coefficients in all three principal components of the rain anomaly. This is undoubtedly due in no small part to the fact that the TRMM record starts in the middle of one of the strongest ENSO warm

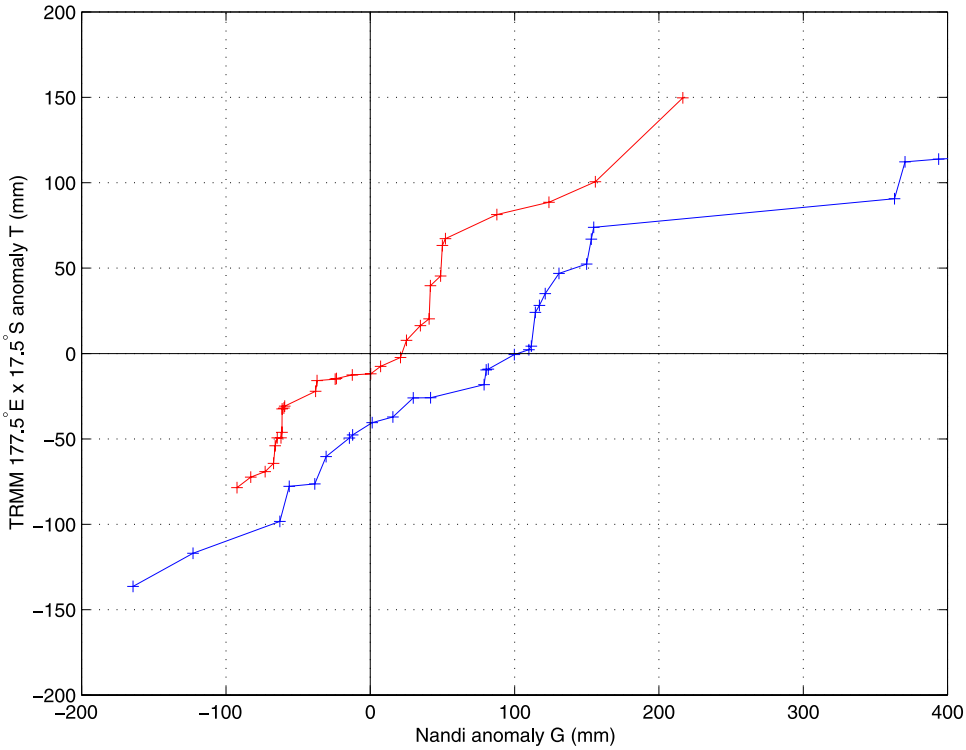

Figure 3. Relations between the ground-station-anomaly G and the TRMM-pixel-anomaly T for Nadi and the pixel centered at 177.5°E 17.5°S (November–April (blue) and May–October (red)).

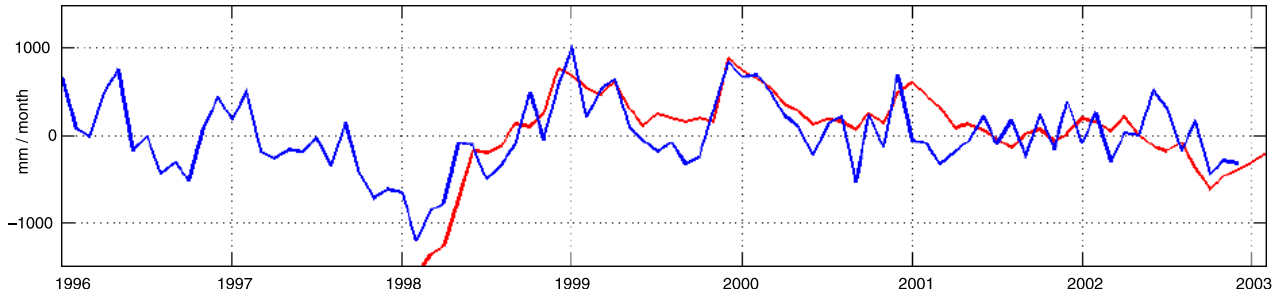

Figure 4. The time series of the TRMM-combined anomaly PC_1 (red) and its 21-station fit PC_1' (blue).

phases of the twentieth century. However, the coefficients of the principal components over the various pixels within the Pacific are not entirely consistent with the ENSO pattern. For example, the PC_1 coefficients over Micronesia/western Pacific region are similar to those over Indonesia/New Guinea, yet Ropelewski and Halpert have shown that while the rain anomalies during low-index ENSO phases are similar in both regions, they differ during high index phases. Similarly, while the PC_1 coefficients over the Fiji/New Caledonia region are consistent with Indonesia/New Guinea, as predicted by *Ropelewski and Halpert*'s [1987, 1988] study, the similarity is less apparent in PC_2 and has totally disappeared in PC_3.

3. Extending the TRMM Record

[6] In order to understand in more detail and eventually quantify how the principal components of the rain anomaly do correlate with the physical mechanisms which directly affect rainfall, it is important to find a way to extend the TRMM observations in general, and the anomaly index PC_1 in particular, beyond the 5 years worth of TRMM data. We

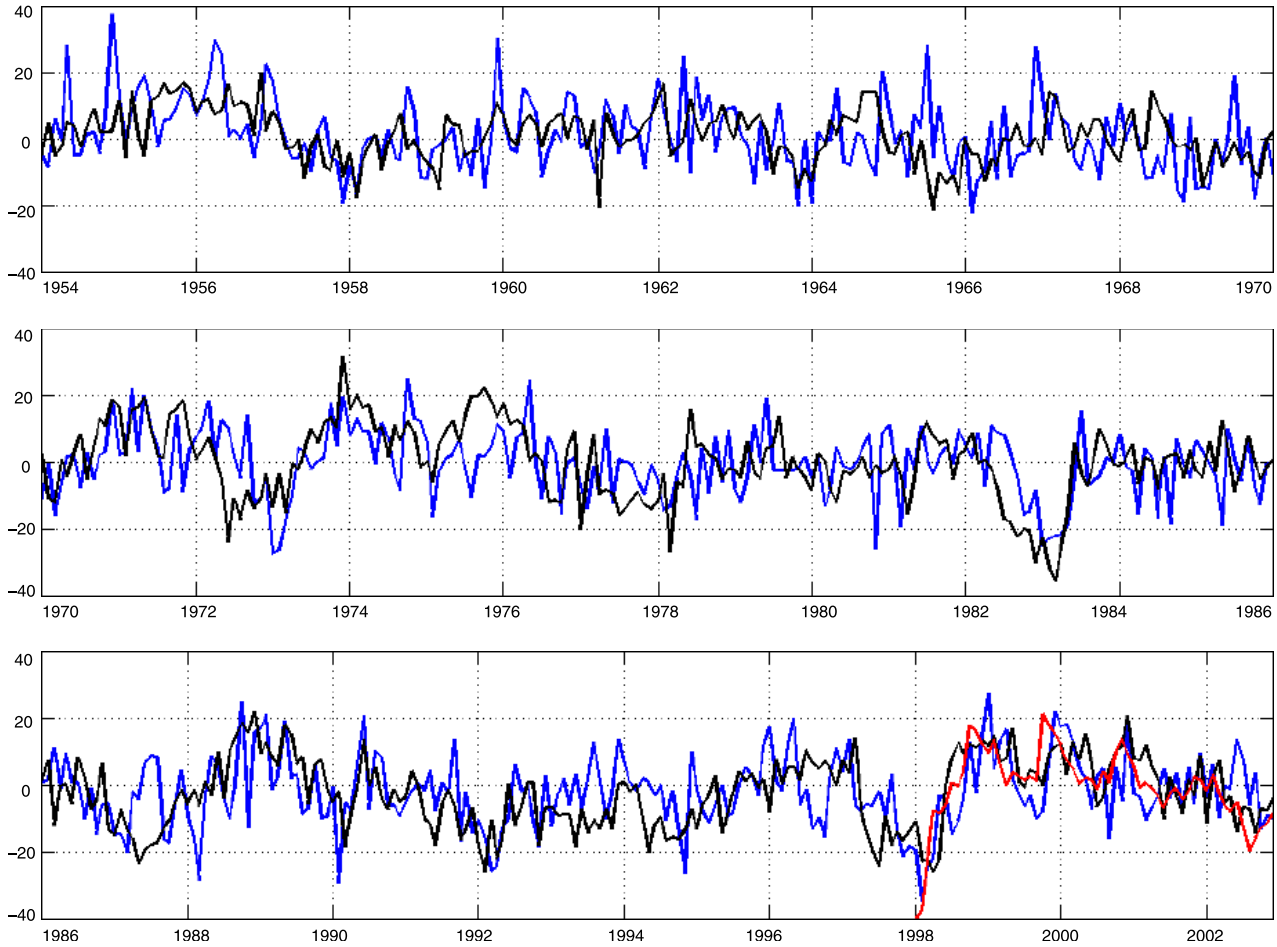

Figure 5. The time series of the TRMM-combined anomaly PC_1 (red), its 21-station fit PC_1' (blue), and the Southern Oscillation Index (black).

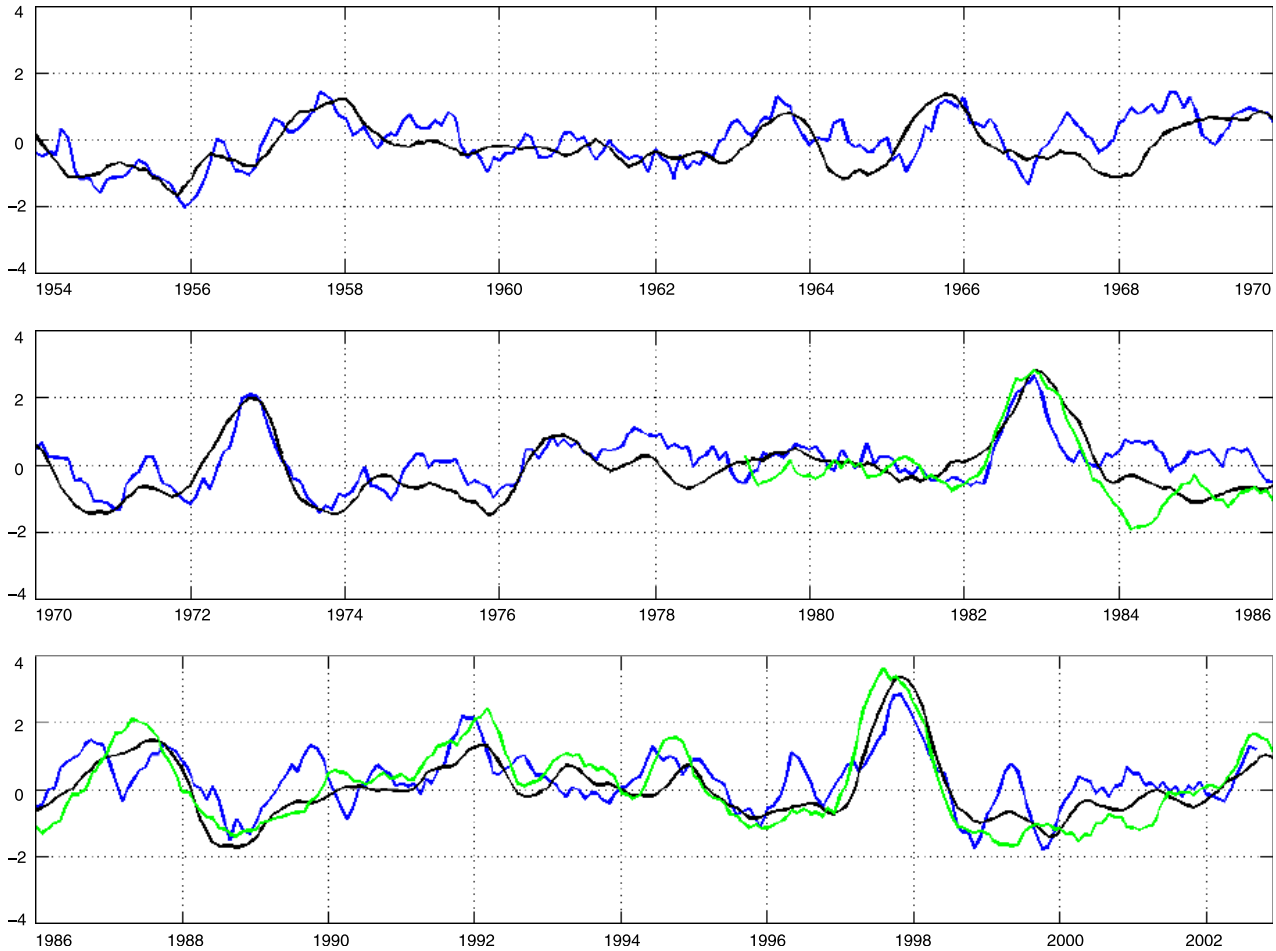

Figure 6. The TRMM-combined anomaly proxy PC_1' (blue), ENSO precipitation index (green), and the Nino-3 index (black).

attempted to achieve this by making use of the Global Historical Climatology Network (GHCN) rainfall data set [*Peterson and Vose*, 1997], which provides monthly surface rain accumulations from over 20,000 surface stations. We started by distinguishing those TRMM pixels whose coefficients in the first three anomaly principal components are large in absolute value, and for which there exists at least one surface station in the GHCN database with a reasonably complete observational record extending to December 2002 (i.e., overlapping the TRMM record) and reaching back at least to the 1950s or earlier. In addition, if a surface station with reliable monthly data from 1954 to 2002 fell in a pixel with a PC_1 coefficient smaller than 0.05 in absolute value, it was retained only if the corresponding PC_2 and PC_3 coefficients were less than 0.03 in absolute value. We thus identified 21 pixels (highlighted in white in Figure 2) and 21 corresponding surface stations, listed in Table 1.

[7] Note that five of these stations are in Micronesia, whose rain anomaly *Ropelewski and Halpert* [1987, 1988] found not to correlate consistently with ENSO. Next, one must account for the fact that the surface station accumulations are not perfectly representative of the amounts TRMM would have estimated over the corresponding pixel. If one had a large amount of 5° × 5° anomaly data $\{T\}$ (normalized relative to the TRMM-combined January 1998 to December 2002 baseline) carefully classified according to the underlying rain regime, along with the corresponding surface station anomalies $\{G\}$ (calculated relative to the same baseline), it would not be unreasonable to postulate a direct relation $T = f(G)$ with f depending on the particular location and the particular rain regime. Under this hypothesis, the best way to estimate f from the data is to match the cumulative distributions of G and T [*Haddad and Rosenfeld*, 1997]. We performed separate probability matches for the 21 stations for each of two seasons, May to October and November to April. The resulting probability-matching functions f are illustrated in Figure 3 for the pixel 177.5°E × 17.5°S represented by the ground station at Nadi, Fiji. Linear fits for all 46 probability-matching G-T relations are shown in Table 1. Using them, we can now define a "proxy" PC_1' for the first TRMM-combined anomaly index PC_1: Indeed, where the latter was a combination $PC_1 = \sum a_n T_n$ over all 1152 pixels, define the proxy to be the sum $PC_1' = c\sum_{n=1}^{21} a_n f_n(G_n)$ over the 21 stations, with the same TRMM-combined coefficients a, and where f_n is the probability-matching station-pixel relation for the nth pixel and the appropriate season (May to October or November to April), and where the sum has to be renormalized by the factor $c = \sqrt{1152/21}$. The comparison between the actual

TRMM-combined index PC_1 and its 21-station proxy PC_1' is shown in Figure 4. The correlation coefficient between the two is 0.87, not perfect but quite reasonable. As Figure 4 suggests, we can now compare PC_1' to any climatological index over the past few decades. The obvious candidates for such a comparison are the ENSO indices, and Figure 5 shows the graphs of PC_1' and the *Troup* [1965] SOI calculated as

$$\mathrm{SOI} = 10\,\frac{[\text{Tahiti SLP} - \text{Darwin SLP}] - \text{mean}}{\text{standard deviation}}$$

where the mean and standard deviation are calculated over the period from 1887 until 1989. The scaling factor $\lambda = 0.027$ which was used to change the units of PC_1' was obtained by minimizing the conditional mean squared distance between $\lambda\, PC_1'$ and SOI, over those months where SOI exceeds 1.5 times its standard deviation (in order to avoid fitting noise). The correlation coefficient was 0.65, and this already respectable value exceeds 0.7 if the correlation is calculated only for those samples where either index exceeds 1.8 times the standard deviation of SOI. Finally, Figure 6 shows the graphs of the 5-month negative running average $\overline{PC}_1'(m) = -PC_1'(m-2) - \cdots - PC_1(m+2)$ for all months m, along with the similarly averaged Nino-3 [see, e.g., *Trenberth and Stepaniak*, 2001], and ESPI indices. In this case, the (unconditional) correlation between the time series Nino-3(y) and $\overline{PC}_1'(y+t)$ reaches a maximum of 0.68 when $t = 2$ months. The same $t = 2$ months delay applied to $\overline{PC}_1'(y+t)$ maximizes its correlation with ESPI(y) at the slightly lower value of 0.65. These results confirm that the global rain anomaly is well correlated with ENSO.

[8] Thus one can conclude that the TRMM record confirms that ENSO is the major driver of the interannual variability of global rainfall. It is indeed remarkable that, although the TRMM data encompass a single major negative ENSO phase, the first-order global measure of its anomaly PC_1 captures enough of the characteristics of ENSO that its extension back in time PC_1' correlates quite well with the well-established ENSO indices over five decades. This result relies on the validity of the TRMM data. While to date the latter have not been shown to have significant biases, the additive white noise in the instantaneous rain estimates is substantial, and does not entirely disappear when spatial and temporal averages are taken. However, since the principal component analysis is linear, this uncertainty does not affect the expected value of the principal components and cannot affect the high correlation between PC_1' and the ENSO indices.

[9] These conclusions should be tempered by three observations. The first is that the record of TRMM estimates of surface rainfall is geographically restricted to latitudes between 40°S and 40°N. Future precipitation remote sensing projects, such as the multinational Global Precipitation Measurement mission's plans for a constellation of satellites, should extend the coverage to a much greater proportion of the globe. The second observation is that our method of extending TRMM's 60-month record to the preceding decades is admittedly approximate and could be greatly improved with the advent of higher-resolution global models. Finally, the principal component analysis does highlight those regions where the installation of denser networks of precise in situ rainfall-measuring instruments would be most cost-effective in validating the estimates of future remote-sensing missions as well as those of enhanced weather models.

[10] **Acknowledgment.** This work was performed at the Jet Propulsion Laboratory, California Institute of Technology, under contract with the National Aeronautics and Space Administration.

References

Adler, R. F., A. J. Negri, P. R. Keehn, and I. M. Hakkarinen (1993), Estimation of monthly rainfall over Japan and surrounding waters from a combination of low-orbit microwave and geosynchronous IR data, *J. Appl. Meteorol.*, *32*, 335–356.

Adler, R. F., G. J. Huffman, D. T. Bolvin, S. Curtis, and E. J. Nelkin (2000), Tropical rainfall distributions determined using TRMM combined with other satellite and rain gauge information, *J. Appl. Meteorol.*, *39*, 2007–2023.

Arkin, P. A. (1979), Relationship between fractional coverage of high cloud and rainfall accumulations during GATE over the B-scale array, *Mon. Weather Rev.*, *107*, 1382–1386.

Curtis, S., and R. F. Adler (2000), ENSO indices based on patterns of satellite-derived precipitation, *J. Clim.*, *13*, 2786–2793.

Dai, A., and I. M. L. Wigley (2000), Global patterns of ENSO-induced precipitation, *Geophys. Res. Lett.*, *27*, 1283–1286.

Dai, A., I. Y. Fung, and A. D. Del Genio (1997), Surface observed global land precipitation variations during 1900–88, *J. Clim.*, *10*, 2943–2962.

Haddad, Z. S., and D. Rosenfeld (1997), Optimality of Z-R relations, *Q. J. R. Meteorol. Soc.*, *123*, 1283–1293.

Haddad, Z. S., E. A. Smith, C. D. Kummerow, T. Iguchi, M. R. Farrar, S. L. Durden, M. Alves, and W. S. Olson (1997), The TRMM day-1 radar/radiometer combined rain-profiling algorithm, *J. Meteorol. Soc. Jpn.*, *75*, 799–809.

Huffman, G. J., R. F. Adler, P. Arkin, A. Chang, R. Ferraro, A. Gruber, J. Janowiak, A. McNab, B. Rudolf, and U. Schneider (1997), The Global Precipitation Climatology Project (GPCP) combined precipitation dataset, *Bull. Am. Meteorol. Soc.*, *78*, 5–20.

Peterson, T. C., and R. S. Vose (1997), An overview of the global historical climatology network temperature database, *Bull. Am. Meteorol. Soc.*, *78*, 2837–2849.

Ropelewski, C. F., and M. S. Halpert (1987), Global and regional scale precipitation patterns associated with the El-Niño Southern Oscillation, *Mon. Weather Rev.*, *115*, 1606–1626.

Ropelewski, C. F., and M. S. Halpert (1988), Precipitation patterns associated with the high index phase of the Southern Oscillation, *J. Clim.*, *2*, 184–268.

Simpson, J., R. F. Adler, and G. R. North (1988), A proposed Tropical Rainfall Measuring Mission (TRMM) satellite, *Bull. Am. Meteorol. Soc.*, *69*, 278–295.

Trenberth, K. E., and D. P. Stepaniak (2001), Indices of El Niño evolution, *J. Clim.*, *14*, 1697–1701.

Troup, A. J. (1965), Southern oscillation, *Q. J. R. Meteorol. Soc.*, *91*, 490–491.

Xie, P., and P. A. Arkin (1997), Global precipitation: A 17-year monthly analysis based on gauge observations, satellite estimates, and numerical model outputs, *Bull. Am. Meteorol. Soc.*, *78*, 2539–2558.

R. F. Adler and E. A. Smith, NASA Goddard Space Flight Center, Greenbelt, MD 20771, USA.

S. L. Durden, Z. S. Haddad, E. Im, and J. P. Meagher, Jet Propulsion Laboratory, 4800 Oak Grove Drive, California Institute of Technology, Pasadena, CA 91109, USA. (zsh@titan.jpl.nasa.gov)